

## Three-beam interference lithography methodology

J. L. Stay, G. M. Burrow, and T. K. Gaylord

Citation: *Rev. Sci. Instrum.* **82**, 023115 (2011); doi: 10.1063/1.3535557

View online: <http://dx.doi.org/10.1063/1.3535557>

View Table of Contents: <http://rsi.aip.org/resource/1/RSINAK/v82/i2>

Published by the [American Institute of Physics](#).

---

### Related Articles

High performance broadband absorber in the visible band by engineered dispersion and geometry of a metal-dielectric-metal stack

*Appl. Phys. Lett.* **101**, 241116 (2012)

Selectively grown photonic crystal structures for high efficiency InGaN emitting diodes using nanospherical-lens lithography

*Appl. Phys. Lett.* **101**, 211111 (2012)

Lithographically defined low dimensional SiGe nanostripes as silicon stressors

*J. Appl. Phys.* **112**, 094318 (2012)

Note: Controlled fabrication of suspended metallic vacuum tunneling gaps

*Rev. Sci. Instrum.* **83**, 106108 (2012)

Liquid-like instabilities in gold nanowires fabricated by focused ion beam lithography

*Appl. Phys. Lett.* **101**, 163108 (2012)

---

### Additional information on Rev. Sci. Instrum.


Journal Homepage: <http://rsi.aip.org>

Journal Information: [http://rsi.aip.org/about/about\\_the\\_journal](http://rsi.aip.org/about/about_the_journal)

Top downloads: [http://rsi.aip.org/features/most\\_downloaded](http://rsi.aip.org/features/most_downloaded)

Information for Authors: <http://rsi.aip.org/authors>

## ADVERTISEMENT



**JANIS**

Does your research require low temperatures? Contact Janis today.  
Our engineers will assist you in choosing the best system for your application.

10 mK to 800 K	LHe/LN <sub>2</sub> Cryostats
Cryocoolers	Magnet Systems
Dilution Refrigerator Systems	
Micro-manipulated Probe Stations	

**sales@janis.com    www.janis.com**  
**Click to view our product web page.**

## Three-beam interference lithography methodology

J. L. Stay, G. M. Burrow, and T. K. Gaylord

*School of Electrical and Computer Engineering, Georgia Institute of Technology,  
Atlanta, Georgia 30332-0250, USA*

(Received 22 October 2010; accepted 10 December 2010; published online 24 February 2011)

Three-beam interference lithography represents a technology capable of producing two-dimensional periodic structures for applications such as micro- and nanoelectronics, photonic crystal devices, metamaterial devices, biomedical structures, and subwavelength optical elements. In the present work, a systematic methodology for implementing optimized three-beam interference lithography is presented. To demonstrate this methodology, specific design and alignment parameters, along with the range of experimentally feasible lattice constants, are quantified for both hexagonal and square periodic lattice patterns. Using this information, example photonic crystal rodlike structures and hole-like structures are fabricated by appropriately controlling the recording wavevector configuration along with the individual beam amplitudes and polarizations, and by changing between positive- or negative-type photoresists. © 2011 American Institute of Physics. [doi:[10.1063/1.3535557](https://doi.org/10.1063/1.3535557)]

### I. INTRODUCTION

Multibeam interference lithography (MBIL) can be used to produce a wide variety of one-, two-, and three-dimensional micro- and nanoperiodic structures and is widely recognized as a promising technology with numerous important applications. Major fields of application include (1) micro- and nanoelectronics, (2) photonic crystal devices, (3) metamaterial devices, (4) biomedical structures, and (5) subwavelength optical elements. *Micro- and nanoelectronics* include circuit configurations for devices such as dynamic random access memory (DRAM) which consist of a highly periodic layout of cells with an underlying periodic grid pattern that defines the smallest feature size in these cells.<sup>1</sup> MBIL can be used to define this underlying grid. As such MBIL may serve as a cornerstone for future optical lithography systems. *Photonic crystal devices* offer the potential of truly dense integrated photonic circuits and systems.<sup>2,3</sup> These devices are based on periodic structures that provide a high degree of light confinement through the mechanism of diffraction (rather than through refractive index contrast). Individual components that are being developed include waveguides, resonators, antennas, sensors, multiplexers, filters, couplers, and switches. *Metamaterial devices* have many potentially important commercial applications<sup>4–6</sup> based on periodic structures at a size scale much smaller than the wavelength of light. Metamaterials overcome the natural lack of magnetic dipole in materials through cell structures such as split-ring resonators. The index of refraction, in general, is  $n = \pm(\epsilon_r\mu_r)^{1/2}$ . In a metamaterial when both  $\epsilon_r$  and  $\mu_r$  are less than zero, the refractive index is negative. Applications include ultracompact objective lenses, frequency-doubling devices, parametric amplifiers, and parametric oscillators. *Biomedical structures* that are periodic or quasiperiodic in one-, two-, and three-dimensions are critically important in a wide variety of areas. For example, in regenerating nerves, arrays of microchannels are needed to guide nerve growth.<sup>7</sup> In facilitating bone regrowth, periodic meshes are needed to retain and sequester bone mor-

phogenetic protein.<sup>8</sup> In the forming, maintaining, and repairing of tissue, engineered surfaces are needed that present controlled densities of peptides to direct assembly of extracellular matrices.<sup>9</sup> *Subwavelength optical elements* utilize high spatial frequency periodic structures. These subwavelength-based optical elements fall in three broad categories: (1) synthesized-index elements, (2) form-birefringent polarization elements, and (3) guided-mode resonant elements.<sup>10</sup> Synthesized-index elements include two-dimensional crossed gratings that have been implemented to provide polarization independent antireflection behavior mimicking the effect of a “moth’s eye”<sup>11,12</sup> to increase the efficiency of solar cells.<sup>13,14</sup> A 100 nm period grating in an amorphous silicon thin film has been used to stabilize the linear polarization of vertical-cavity surface-emitting lasers (VCSEL’s).<sup>15</sup> Guided-mode resonant gratings are widely utilized for their very narrowband filter characteristics<sup>16–18</sup> in dense-wavelength-division multiplexed communications and in chemical, biological, toxicological, and environmental sensing applications. For all five applications areas, MBIL is well suited to provide an efficient, inexpensive method of fabricating the required periodic structures.

In the literature, MBIL results are typically presented for unique sets of parameters that produce a specific desired periodic lattice. However, there is frequently little discussion on how these parameters were selected. Further, it is unclear as to what total range of periodic structure parameters might be available for a given published experimental configuration. To move MBIL toward becoming a routinely used technology, a systematic configuration design methodology is needed that provides the needed precise control of design parameters. MBIL experiments are frequently sensitive to the orientations, amplitudes, and polarizations of the individual beams. A systematic procedure to establish correct alignment, amplitude, and polarization is needed. Accompanying this, it is necessary to be able to check the alignment, amplitude, and polarization. An experimental method is needed to check and to maintain the beam parameters. A systematic methodology

for design, for determination of the possible range of parameters, for establishing, checking, and maintaining alignment is missing from the scientific literature.

In the present work, a systematic methodology for implementing optimized three-beam interference lithography is presented. The configuration and procedures presented here were specifically developed to demonstrate experimentally the methodology presented by Stay *et al.* to maximize the absolute contrast while satisfying the conditions for uniform contrast in three-beam interference.<sup>19</sup> In general, the methodology presented here may be applied to other efforts requiring multibeam interference. Specific design and alignment parameters are quantified for optimized hexagonal periodic patterns with  $p6m$  plane group symmetry and square patterns with  $p4m$  plane group symmetry. The range of experimentally feasible lattice constants is presented for both patterns using the configuration described in the present work. A real-time monitoring technique is presented that aids in the validation and production of both rodlike structures and holelike structures that are formed by appropriately controlling the recording wavevector configuration along with the individual beam amplitudes and polarizations, and by changing between positive- or negative-type photoresists. As a demonstration of methodology, both hexagonal and square periodic photonic crystal lattices are fabricated with a single optical lithography exposure (rather than the conventional double exposure technique<sup>20,21</sup>).

## II. SYSTEM DESIGN

### A. Requirements

It has been shown that MBIL can produce all two- and three-dimensional Bravais lattices and 9 of the 17 plane group symmetries.<sup>19,22</sup> Recently, *conditions for primitive-lattice-vector-direction equal contrasts* have been introduced.<sup>19</sup> These conditions require individual control for each recording wavevector,  $\mathbf{k}_i$ , beam amplitude,  $E_i$ , and polarization vector,

$\hat{\mathbf{e}}_i$ , in order to produce an interference pattern with maximized absolute contrast,  $V_{\text{abs}}$ , and uniform contrast in the primitive-lattice-vector directions as required for the desired lattice translational and plane group symmetry. In this method, a symbolic designation,  $\pm C_n^{(m)}$ , is introduced, where the quantity  $n$  is the total number of interfering beams and  $m$  is the number of contributing interfering-beam pairs, where a given beam pair may produce a one-dimensional fringe pattern that contributes to the overall MBIL periodic pattern based on the relative linear polarizations of the individual beams. The sign of the symbolic designation indicates whether an intensity maxima (+) or minima (−) is located at a lattice point. For a hexagonal lattice with  $p6m$  plane group symmetry, the conditions for  $\pm C_3^{(3)}$  must be applied. Similarly,  $\pm C_3^{(2)}$  conditions are required for square lattices with  $p4m$  plane group symmetry. By applying the conditions for  $\pm C_n^{(m)}$  and maximizing absolute contrast to determine the required individual beam parameters, a high-quality, lithographically useful interference pattern is possible. Using this methodology, it is shown that unity absolute contrast,  $V_{\text{abs}} = 1$ , can always be achieved for a square lattice with  $p4m$  plane group symmetry. For the hexagonal lattice with  $p6m$  plane group symmetry, unity absolute contrast can only be achieved when intensity minima are located at lattice points, satisfying the  $-C_3^{(3)}$  conditions. For the  $+C_3^{(3)}$  case,  $V_{\text{abs}}$  varies from a maximum of unity absolute contrast (when all three recording wavevectors are collinear or coplanar) to a minimum optimized absolute contrast of  $V_{\text{abs}} = 0.6$  (when all three recording wavevectors are orthogonal).

### B. Three-beam interference configuration

A configuration to perform optimized three-beam interference satisfying the requirements for individual control of beam direction, amplitude, and polarization was designed, tested, and constructed as depicted in Fig. 1. In this configuration, particular attention is focused on stability, design versatility (in terms of wavevector configurations and control of

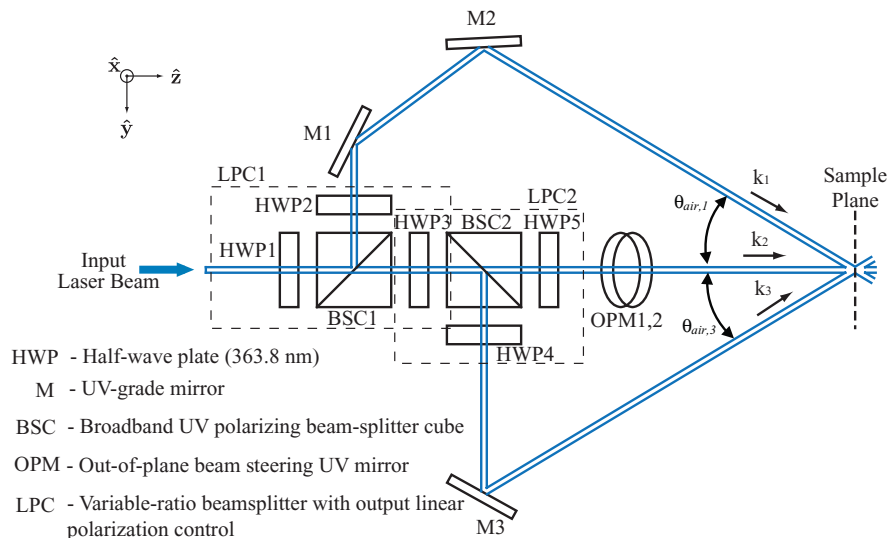


FIG. 1. (Color online) Three-beam interference configuration. The outlined variable-ratio beamsplitters with output linear polarization control (LPC) provide individual control of each interfering beam amplitude and polarization, while the mirrors (M, OPM) provide control of the recording wavevector configuration.

individual beam parameters), reduction of unwanted reflections, and phase front quality.

A Spectra Physics BeamLok 2065-5S argon ion laser is used as the source for this configuration with an etalon and etalon controller providing stable, linearly polarized, single frequency operation at 363.8 nm with frequency jitter of <10 MHz for <1 s and <20 MHz for <2 min for fabrication via interference lithography. Given a value of 20 MHz frequency jitter and exposure times of well under 2 min, this equates to a change in recording wavelength,  $\Delta\lambda$ , of no more than  $\Delta\lambda = 4.41 \times 10^{-6}$  nm over the duration of the exposure. For a hexagonal or square pattern with a lattice constant of  $1.5\lambda$  (545.7 nm), the lattice constant should change by no more than  $\pm 1.3 \times 10^{-6}\%$ . In order for one period of the interference pattern to be completely washed out during an exposure, the sample area would have to be greater than 40 m in diameter. The wavelength stability in this configuration is clearly sufficient.

From a chemistry standpoint, an ultraviolet (UV) based fabrication process source is advantageous due to the wide availability of UV-based lithographic materials. While some groups have fabricated photonic crystal structures using visible light laser sources, these processes require unconventional photoresist formulations to enhance absorption in the visible part of the spectrum.<sup>23–25</sup> Even with this enhancement, relatively large exposure doses are required. By contrast, many photoresists have been designed for operation at 365 nm (mercury i-line) due to the microelectronics industry. The optical lithography recipes for these photoresists are easily adapted by replacing a traditional mask-based exposure with a MBIL exposure.

In order to provide design versatility, individual control of beam amplitude and polarization is accomplished with a variable-ratio beamsplitter with output linear polarization control (LPC) as outlined in Fig. 1. A single LPC stage consists of three half-wave plates (HWP's) and a polarizing beamsplitter cube (BSC), all designed to operate at 363.8 nm. Each half-wave plate rotates the plane of polarization of the input beam about the plane of the crystalline optic axis normal to the surface of the wave plate, thereby eliminating the need to manipulate physically the laser. A polarizing cube beamsplitter (as opposed to a slab beamsplitter) is used to eliminate ghost beams. Each BSC reflects S-polarized light (vertical to table) while transmitting P-polarized light (horizontal to table). The input half-wave plate of an LPC stage rotates the plane of the input linearly polarized light, thereby allowing control over the amplitude,  $E_i$ , of each BSC output wavevector,  $\mathbf{k}_i$ , as depicted in Fig. 1. An additional half-wave plate is placed in the path of each linearly polarized BSC output beam, thereby allowing control over the direction of the linear polarization vector,  $\hat{\mathbf{e}}_i$ , of each wavevector,  $\mathbf{k}_i$ . In the three-beam interference configuration shown in Fig. 1, the half-wave plate in the output path of the transmitted BSC beam of LPC1 is used as the input half-wave plate to LPC2. Using this methodology, it is possible to individually control the amplitude and polarization of each interfering beam.

UV-grade mirrors steer the beams in the appropriate directions according to the recording wavevector,  $\mathbf{k}_i$ , requirements. The optics that compose both LPC stages and mirrors

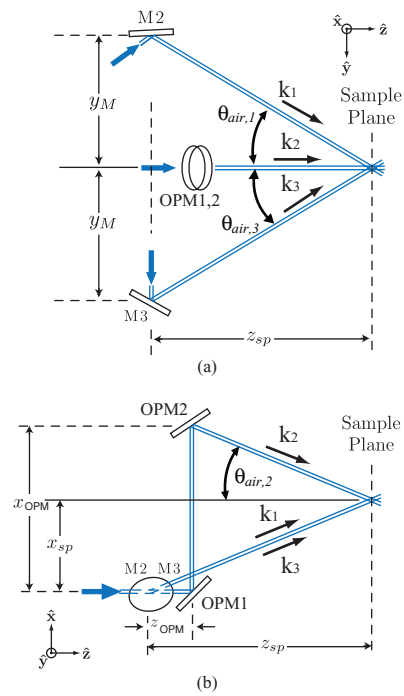


FIG. 2. (Color online) Three-beam interference critical experimental configuration parameters. The critical experimental parameters are illustrated in the (a) top view and (b) side view of the configuration.

M1, M2, and M3 are set at a common height above the optical table equal to that of the input laser beam. Mirrors M2 and M3 control the incident angle upon the sample plane with respect to the  $z$  axis,  $\theta_{\text{air},1}$  and  $\theta_{\text{air},3}$  of wavevectors  $\mathbf{k}_1$  and  $\mathbf{k}_3$ , respectively, as depicted in Fig. 1. The first out-of-plane beam steering mirror (OPM1) in the path of beam 2 is set at the common height above the optical table equal to that of the input laser beam and adjusted such that the beam is reflected perpendicularly to the optical table as depicted in Fig. 1. The second mirror OPM2 is set at a variable height above OPM1 and adjusted to control the incident angle,  $\theta_{\text{air},2}$ , for wavevector  $\mathbf{k}_2$  as depicted in Fig. 2. With this configuration, all of the wavevector configurations required for the fabrication of one- and two-dimensional periodic patterns are possible via single exposure. Three-dimensional patterns are possible with multiple exposures. Alternatively, an additional LPC stage can be incorporated into this configuration to add a fourth interfering beam, allowing for single exposure, four-beam interference for fabrication of three-dimensional periodic patterns.

In order to create a hexagonal interference pattern with  $p6m$  plane group symmetry and high absolute contrast,  $V_{\text{abs}}$ , the polarizations and amplitudes of the recording beams are adjusted accordingly. Given the two fundamentally different types of interference patterns,  $+C_3^{(3)}$  and  $-C_3^{(3)}$ , and the different indices of refraction,  $n_{\text{PR}}$ , of the two recording media (1.736 for the Shipley 1813 positive resist and 1.58 for the Futurrex NR7-1500P negative resist), there are four distinct optimal configurations for the polarizations and beam amplitudes and two recording wavevector configurations, one for each resist. Each beam at a common free-space incidence angle,  $\theta_{\text{air}}$ , as depicted in Figs. 1 and 2) is refracted at the air-photoresist interface, changing the common



TABLE I. Summary of optimized beam parameters and resulting absolute contrast for a hexagonal interference pattern (lattice constant  $a = 1.5\lambda$ ) with  $p6m$  plane group symmetry defined in Shipley 1813 and Futurrex NR7–1500P photoresists.

Parameter	Shipley 1813		Futurrex NR7–1500P	
$\theta_{PR}$	14.83°		16.34°	
$\mathbf{k}_1/(n_{PR}\mathbf{k}_0)$	[0.13 0.22 0.97]		[0.14 0.24 0.96]	
$\mathbf{k}_2/(n_{PR}\mathbf{k}_0)$	[−0.26 0 0.97]		[−0.28 0 0.96]	
$\mathbf{k}_3/(n_{PR}\mathbf{k}_0)$	[0.13 −0.22 0.97]		[0.14 −0.24 0.96]	
	$+C_3^{(3)}$	$-C_3^{(3)}$	$+C_3^{(3)}$	$-C_3^{(3)}$
$E_2/E_1$	−1.08		−1.09	
$E_3/E_1$	1		1	
$\hat{\mathbf{e}}_1$	[−0.99 0.04 0.12]		[−0.99 0.05 0.13]	
$\hat{\mathbf{e}}_2$	[0.97 0 0.26]		[0.96 0 0.28]	
$\hat{\mathbf{e}}_3$	[−0.99 −0.04 0.12]		[−0.99 −0.05 0.13]	
$\psi_{x,1}$	−88.68°		−89.11°	
$\psi_{x,2}$	90°		90°	
$\psi_{x,3}$	−91.32°		−90.89°	
$V_{abs}$	0.96		0.96	

incidence angle in the photoresist,  $\theta_{PR}$ , as described by Snell's Law,  $n_{air} \sin(\theta_{air}) = n_{PR} \sin(\theta_{PR})$ . Since the sample is placed normal to the  $z$  axis, both the common incidence angle and the source wavelength are altered such that the lattice constant of the periodic pattern in the photoresist is the same as that of the free-space periodic pattern. Similarly, the amplitudes,  $E_i$ , of the each beam do not change at the air–photoresist interface. However, the polarization vectors,  $\hat{\mathbf{e}}_i$ , contained in the plane normal to the wavevector, do change within the photoresist. Accordingly, the calculated free-space polarization vectors are adjusted such that the refracted beam polarization vectors are optimized within the photoresist.

In order to facilitate the accurate adjustment of the free-space polarizations for each beam, a rotation angle,  $\psi_{x,i}$ , is calculated with respect to  $\hat{\mathbf{x}} \times \mathbf{k}_i$  via a counterclockwise angular rotation (when looking antiparallel to the wavevector  $\mathbf{k}_i$ ) where  $\psi_{x,i} = 0$  and  $\hat{\mathbf{e}}_{x,i} = \hat{\mathbf{x}} \times \mathbf{k}_i$ . This parameter is useful since the polarization direction of  $\psi_{x,i} = 0$  is parallel to the optics table, and thus straightforward to locate and adjust experimentally. Using the calculated value for  $\psi_{x,i}$ , a Glan–Thompson polarizer is placed in the path of each recording beam (after the beam directing mirrors) and the axis of polarization is rotated to  $\psi_{x,i} + \pi/2$ . A power meter is used to monitor the beam after the polarizer as the output half-wave plate for the appropriate LPC stage (HWP2 for beam 1, HWP5 for beam 2, HWP4 for beam 3) is rotated until the beam intensity is minimized.

It should be noted that the beam steering mirrors, though low loss, do alter the polarizations the individual beams based the phase difference of the orthogonal polarization components of the reflected beam, making the polarization of the reflected beam slightly elliptical. However, the procedures for adjusting the polarization of the BSC output beams effectively align the semi-major axis of any elliptical polarization with the desired linear polarization vector,  $\hat{\mathbf{e}}_i$ , thereby allowing for optimized interference patterns that accurately represent the desired lattice translational and plane group symmetry.

The four solutions for the optimized beam parameters and resulting absolute contrast for a hexagonal interference pattern with  $p6m$  plane group symmetry are summarized in

Table I. The solutions for a square interference pattern with  $p4m$  plane group symmetry are listed in Table II.

### C. Alignment procedures

Initial alignment parameters for the three-beam configuration depicted in Fig. 1 are obtained from design plots that illustrate the relationships between critical experimental configuration parameters for a given periodic lattice translational symmetry. Areas of experimental feasibility are shaded within each of these plots depicting the range of periodic pattern lattice constants that can be fabricated given the physical constraints of the configuration: size of optomechanics, size of optics table, etc. For the present configuration, there are five critical experimental configuration parameters. These are the perpendicular distance from the optical axis ( $z$  axis) to mirrors M2 and M3,  $y_M$ , the distance along the optic axis from mirror M2 and M3 to the sample plane,  $z_{sp}$ , the distance along the optic axis from mirror M2 and M3 to mirrors OPM1–2,  $z_{OPM}$ , the perpendicular distance above the plane containing

TABLE II. Summary of optimized beam parameters and resulting absolute contrast for a square interference pattern (lattice constant  $a = 1.5\lambda$ ) with  $p4m$  plane group symmetry defined in Shipley 1813 and Futurrex NR7–1500P photoresists.

Parameter	Shipley 1813 $+C_3^{(2)}$	Futurrex NR7–1500P $+C_3^{(2)}$
$\theta_{PR}$	15.75°	17.36°
$\mathbf{k}_1/(n_{PR}\mathbf{k}_0)$	[0 0.27 0.96]	[0 0.30 0.95]
$\mathbf{k}_2/(n_{PR}\mathbf{k}_0)$	[−0.27 0 0.96]	[−0.30 0 0.95]
$\mathbf{k}_3/(n_{PR}\mathbf{k}_0)$	[0 −0.27 0.96]	[0 −0.30 0.95]
$E_2/E_1$	$\sqrt{2}$	$\sqrt{2}$
$E_3/E_1$	1	1
$\hat{\mathbf{e}}_1$	[0.23 −0.94 0.26]	[0.96 −0.26 0.08]
$\hat{\mathbf{e}}_2$	[0.84 −0.48 0.24]	[0.84 0.48 0.26]
$\hat{\mathbf{e}}_3$	[0.96 0.26 0.07]	[0.22 0.93 0.29]
$\psi_{x,1}$	−88.68°	−89.11°
$\psi_{x,2}$	90°	90°
$\psi_{x,3}$	−91.32°	−90.89°
$V_{abs}$	1	1

the input laser beam and normal to the  $x$  axis to OPM2,  $x_{\text{OPM}}$ , and the perpendicular distance above the plane containing the input laser beam to sample plane spot,  $x_{\text{sp}}$ . These critical experimental configuration parameters are labeled in Fig. 2. An additional parameter of interest is the incident angle of the recording beams on the sample plane with respect to the  $z$  axis,  $\theta_{\text{air}}$ . This parameter is needed in order to calculate the optimized plane wave parameters as previously discussed.

All five critical experimental configuration parameters are relevant when aligning the configuration for a two-dimensional hexagonal lattice. For a two-dimensional square lattice, only four parameters are relevant as beams 1 and 3 are adjusted to be parallel to the optics table by setting  $x_{\text{sp}} = 0$ . For both configurations, a restriction is placed upon  $z_{\text{OPM}}$ . This is done because the lattice constant,  $a$ , is a function of  $y_M$ ,  $x_{\text{OPM}}$ , and  $z_{\text{OPM}}$ . Since this four-dimensional relationship is difficult to visualize, the polarization optics and beam steerer are placed as close as possible, resulting in a value of  $z_{\text{OPM}} = 7.62$  cm. The relationships between the remaining four critical experimental configuration parameters for the hexagonal lattice are

$$a/\lambda = 2/[3 \sin(\theta_{\text{air}})], \quad (1)$$

$$\tan(\pi/6) = x_{\text{sp}}/y_M, \quad (2)$$

$$\tan(\theta_{\text{air}}) = [y_M \tan(\pi/3) - x_{\text{sp}}]/z_{\text{sp}}, \quad (3)$$

$$\tan(\theta_{\text{air}}) = (x_{\text{OPM}} - x_{\text{sp}})/(z_{\text{sp}} - z_{\text{OPM}}). \quad (4)$$

Similar geometric relationships are also defined for the square lattice using

$$a/\lambda = 1/[\sqrt{2} \sin(\theta_{\text{air}})]. \quad (5)$$

These relationships are illustrated in Figs. 3 and 4. Given these design constraints, a lattice constant of  $a = 1.5\lambda$

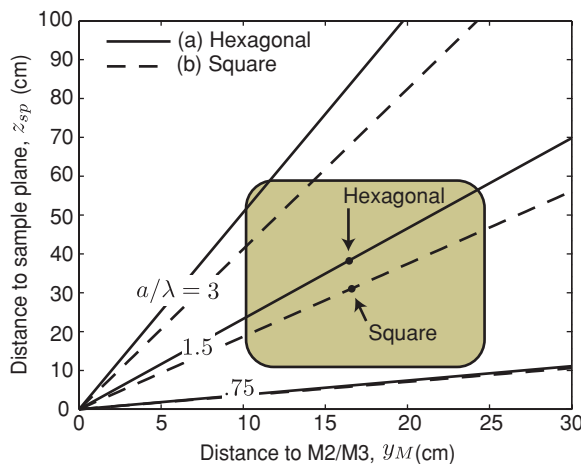


FIG. 3. (Color online) Design plot for aligning the recording beams needed to create two-dimensional (a) hexagonal and (b) square interference patterns. The relationship between the critical experimental configuration parameters  $y_M$ ,  $z_{\text{sp}}$ , and  $a$  is illustrated. The shaded area represents the range of experimental feasibility. The design used in the present work is marked with a solid dot on the plot.

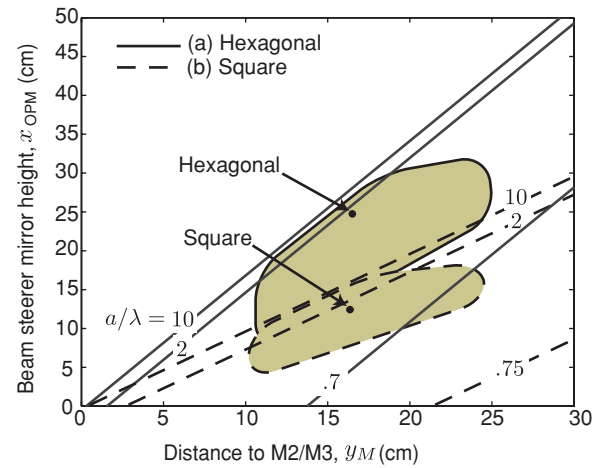


FIG. 4. (Color online) Design plot for aligning the recording beams needed to create two-dimensional (a) hexagonal and (b) square interference patterns. The relationship between the critical experimental configuration parameters  $y_M$ ,  $x_{\text{OPM}}$ , and  $a$  is illustrated. The shaded area represents the range of experimental feasibility. The design used in the present work is marked with a solid dot on the plot.

(545.7 nm) was chosen and marked with a solid dot in the design plots. The values of the resulting critical experimental configuration parameters are listed in Table III. These values are used as the initial alignment parameters for the three-beam interference configuration in the present work.

Fine adjustment of the recording beams is facilitated by the use of an alignment card specifically designed and fabricated for the desired periodic lattice translational symmetry. The alignment cards for a hexagonal lattice and a square lattice are shown in Figs. 5(a) and 5(b), respectively. The alignment card required for a hexagonal lattice includes three alternating holes (approximately the diameter of the laser beam) and three alignment marks (crosses) creating an equilateral regular hexagon. The alignment card required for a square lattice includes three holes and an alignment mark (cross) creating a square. To use the alignment cards, a mirror is placed at the sample plane at a height equal to the calculated sample plane spot height,  $x_{\text{sp}}$ . The alignment card is then positioned at a calculated distance from the mirror. Mirrors M2, M3, and OPM2 are then adjusted such that each beam passes through the appropriate hole on the alignment card, reflects off the mirror in the sample plane, and projects on to the

TABLE III. Critical experimental configuration and alignment parameters and incident angle of the recording beams on the sample plane  $\theta_{\text{air}}$  for a hexagonal and square lattice.

Parameter	Hexagonal lattice value	Square lattice value
$a/\lambda$	1.5	1.5
$y_M$	16.51 cm	16.51 cm
$z_{\text{sp}}$	38.43 cm	30.89 cm
$x_{\text{sp}}$	9.53 cm	0 cm
$x_{\text{OPM}}$	24.82 cm	12.44 cm
$D$	5.08 cm	5.08 cm
$z_{\text{ac}}$	5.12 cm	4.75 cm
$\theta_{\text{air}}$	26.39°	28.13°

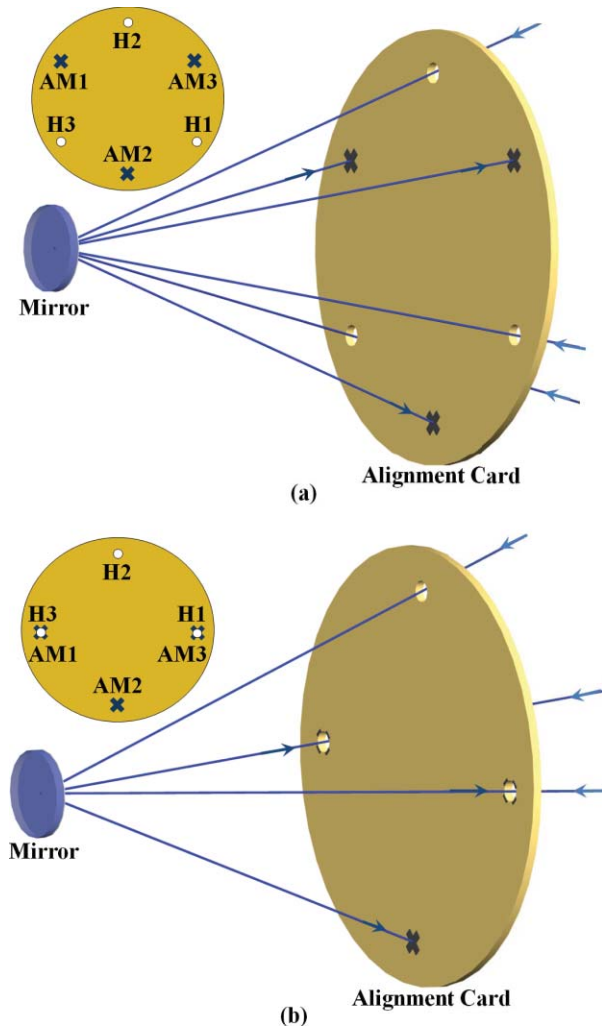


FIG. 5. (Color online) Alignment card used to facilitate fabrication of two-dimensional (a) hexagonal and (b) square lattices. The multibeam-interference configuration is adjusted such that the three separate beams pass through holes H1, H2, and H3, reflect onto the mirror and project onto alignment marks AM1, AM2, and AM3, respectively.

appropriate alignment mark. For the hexagonal lattice, this procedure guarantees three rotationally symmetric beams with respect to the optic. For the square lattice, this procedure guarantees that the projections of beams 1 and 3 are collinear of which the projection of beam 2 is orthogonal to the other two.

Given the diameter of the circumscribed circle of the hexagon or square,  $D$ , and the distance from the alignment card to the mirror,  $z_{ac}$ , the lattice constant of the interference pattern is calculated as

$$a = (2\lambda/3D) \sqrt{D^2 + 4z_{ac}^2} \quad (\text{hexagonal}), \quad (6)$$

$$a = (\sqrt{2}\lambda/2D) \sqrt{D^2 + 4z_{ac}^2} \quad (\text{square}). \quad (7)$$

The positioning of the alignment card is performed with the aid of Fig. 6. This plot illustrates the relationship between the distance separating the mirror and the alignment card,

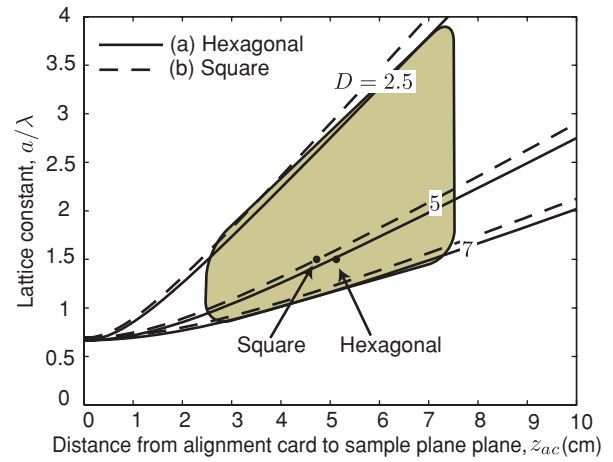


FIG. 6. (Color online) Design plot for aligning the recording beams needed to create two-dimensional (a) hexagonal and (b) square interference patterns. The relationship between the critical experimental configuration parameters  $z_{ac}$ ,  $D$ , and  $a$  is illustrated. The shaded area represents the range of experimental feasibility. The design used in the present work is marked with a solid dot on the plot.

$z_{ac}$ , the diameter of the circumscribed circle of the hexagon,  $D$ , on the alignment card, and the lattice constant,  $a$ . In the present work, a diameter of the circumscribed circle on the alignment card of  $D = 5.08$  cm is used resulting in a distance separating the mirror and the alignment card of  $z_{ac} = 5.12$  and  $4.75$  cm for the hexagonal and square lattices, respectively. All relevant configuration and alignment parameters, including the angle of incidence on the sample plane,  $\theta_{air}$ , are summarized in Table III.

For experimental fabrication purposes, the diameter of the interfering beams at the sample plane remained unchanged from that of the source laser, approximately  $1.7$  mm. However, one of the advantages of an MBIL fabrication is the ability to create large-area, wafer-scale, periodic patterns with a single exposure. In order to expand the area of interference at the sample plane, the beams should be collimated to the desired beam width prior to final adjustment of the recording beams. The final alignment procedures presented in this paper remain unchanged for the collimated beams, noting that the amplitude of light passing through the alignment holes depicted in Fig. 5 would be reduced as a portion of the light incident on the alignment card would be blocked. It is also noted that the exposure time would increase accordingly in order to satisfy the required exposure density of a given photoresist.

### III. SYSTEM PERFORMANCE

#### A. Real-time monitoring

It has been reported that a microscope objective can be used to record the intensity pattern resulting from multibeam interference by placing a photosensitive film directly after the objective for pattern “magnification.”<sup>26</sup> In practice, a microscope objective placed at the sample plane such that the interfering beams enter at the front lens assembly serves two



purposes. One, the interfering beam diameters are increased, thus producing an increased area of interference. Two, the incidence angles of the recording beams,  $\theta_{\text{air}}$ , are decreased, thus increasing the lattice constant of the resulting interference pattern in accordance with Eqs. (1) and (5). With advances in digital image capture devices, real-time monitoring of this “magnified” pattern is readily possible. For the configuration presented in the present work, a Newport microscope objective lens with a 0.85 numerical aperture (NA) and 2.9 mm focal length (60 $\times$ ) provides sufficient “magnification” and acceptance angle for the designs considered. Next, a cooled 3.2 Megapixel Olympus Q-Color3 imaging system digital charge-coupled device (CCD) camera is placed after the microscope objective a distance away such that the CCD array is illuminated by the intersecting area of all three recording beams.

This real-time monitoring system is invaluable in terms of stability analysis, confirmation of translational symmetry, confirmation of group symmetry, and general design verification. Interference patterns may be monitored in real-time, observing the effects of adjustments to individual beam amplitude or polarization, allowing preliminary experimental validation of theories or designs before beginning the more time-consuming fabrication process.

It should be noted that the interference pattern imaged using the CCD camera differs from the interference pattern produced at the sample plane. The microscope objective changes the relative orientation of both the recording wavevectors and the polarizations that are used to create the interference pattern on the CCD array. However, for the design considerations, the real-time monitoring still provides useful information. Specifically, the translational symmetry of the lattice (e.g., two-dimensional square lattice, two-dimensional hexagonal lattice) does not change during imaging. Additionally, a correctly configured multibeam-interference experiment will still result in an image with high contrast.

## B. Fabricated examples

Existing optical lithography recipes for Shipley 1813 positive photoresist were adapted for exposure and development on a UV-grade fused silica substrate using the configuration described in the present work. Once developed, a thin layer (15 nm) of copper was sputtered on the samples for imaging with a Zeiss scanning electron microscope (SEM) Ultra60. Figure 7 depicts fabricated examples of hexagonal rod and hole patterns using the recording and alignment parameters listed in Tables I–III for the Shipley 1813 positive photoresist,  $-C_3^{(3)}$  case.

Figure 8 depicts fabricated examples of square rod and hole lattice patterns using Shipley 1813 positive photoresist defined by an optimized  $+C_3^{(2)}$  interference pattern. For this example, the common incident angle of the recording beams on the sample plane was set to  $\theta_{\text{air}} = 19.19^\circ$  producing a lattice constant of  $a = 782.6$  nm ( $a/\lambda = 2.15$ ). All recording and alignment parameters were adjusted accordingly to optimize absolute contrast for the required symmetry.

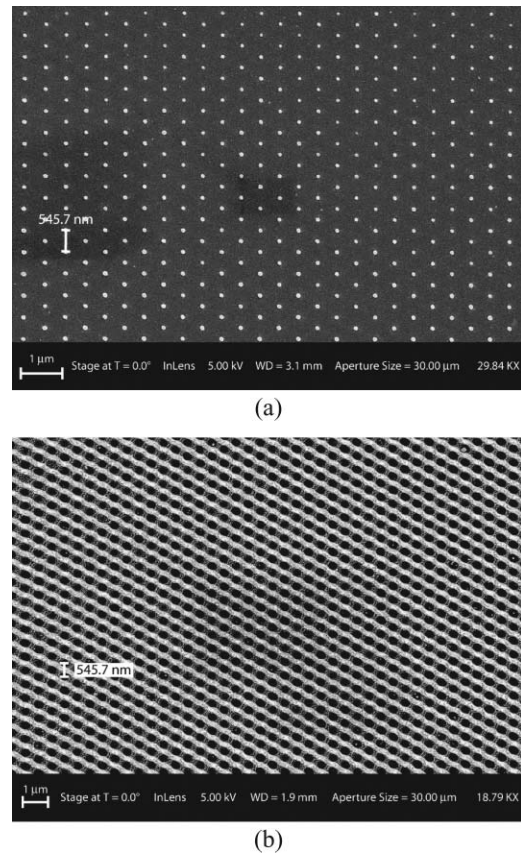


FIG. 7. SEM of hexagonal photonic crystal of (a) rods (lattice constant  $a = 545.7$  nm, rod radius  $r \approx 0.115a \approx 63$  nm) and (b) holes (lattice constant  $a = 545.7$  nm, hole radius  $r \approx 0.30a \approx 166$  nm) defined by three-beam-interference lithography. Shipley 1813 positive photoresist is defined by a  $-C_3^{(3)}$  interference pattern, developed, and copper sputtered.

## IV. DISCUSSION

A methodology for implementing MBIL has been presented. The role of each design and alignment parameter was quantified for both hexagonal and square periodic lattice patterns, along with the associated range of experimentally feasible lattice constants. An experimental procedure for establishing, checking, and maintaining beam alignment in real time was presented. The methodology includes an approach for stabilizing the interference pattern while providing independent control of recording beam parameters for design versatility. Both rodlike structures and holelike structures were fabricated by specifically controlling the recording wavevector configuration along with the individual beam amplitudes and polarizations. To demonstrate the methodology, for the first time to the best of the authors' knowledge, square lattice photonic crystal structures were fabricated with a single optical lithography exposure.

The methodology can be applied to two-beam interference lithography used for producing a wide variety of one-dimensional gratings. Additionally, the configuration may be modified with the additional of a third LPC stage to accommodate four-beam interference lithography used for fabricating three-dimensional periodic structures. The methodology would be compatible with silicon double inversion.<sup>11</sup>



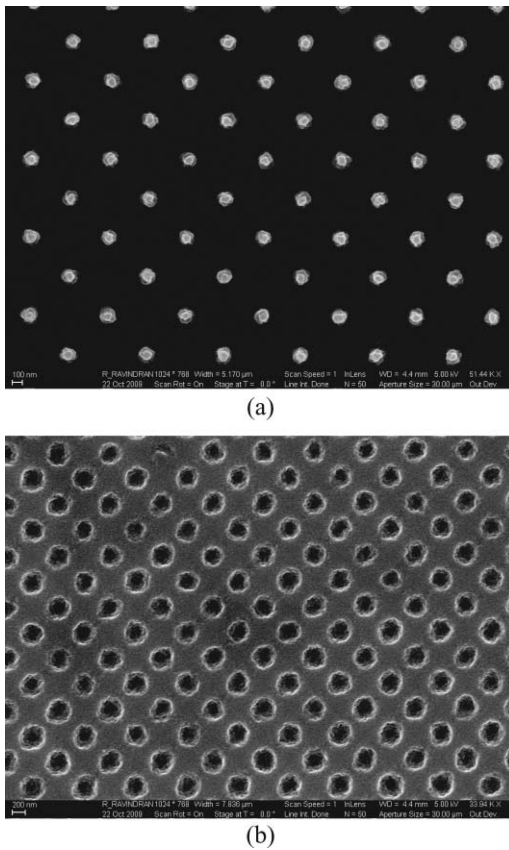


FIG. 8. SEM of square photonic crystal of (a) rods (lattice constant  $a = 782.6$  nm, rod radius  $r \approx 0.18a \approx 138$  nm) and (b) holes (lattice constant  $a = 782.6$  nm, hole radius  $r \approx 0.36a \approx 285$  nm) defined by three-beam-interference lithography. Shipley 1813 positive photoresist was defined by an optimized  $+C_3^{(2)}$  interference pattern, developed, and copper sputtered.

Similarly, the methodology can be applied to N-beam interference lithography.

## ACKNOWLEDGMENTS

This work was supported in part by Grant No. ECCS 0925119 from the National Science Foundation.

- <sup>1</sup>C. A. Mack, *Fundamental Principles of Optical Lithography: The Science of Microfabrication* (Wiley, Chichester, West Sussex, England, 2007).
- <sup>2</sup>H. O. Everitt, *Opt. Photonics News* **3**, 20 (1992).
- <sup>3</sup>G. Parker and M. Charlton, *Phys. World* **13**, 29 (2000).
- <sup>4</sup>M. W. Klein, C. Enkrich, M. Wegener, and S. Linden, *Science* **313**, 502 (2006).
- <sup>5</sup>J. B. Pendry, A. J. Holden, D. J. Robbins, and W. J. Stewart, *IEEE Trans. Microwave Theory Tech.* **47**, 2075 (1999).
- <sup>6</sup>J. B. Pendry and S. D. R., *Sci. Am.* **295**, 60 (2006).
- <sup>7</sup>P. A. Wieringa, R. W. F. Wiertz, E. L. de Weerd, and W. L. C. Rutten, *Proc. IEEE* **98**, 389 (2010).
- <sup>8</sup>M. P. Lutolf, F. E. Weber, H. G. Schmoekel, J. C. Schense, T. Kohler, R. Muller, and J. A. Hibbell, *Nat. Biotechnol.* **21**, 513 (2003).
- <sup>9</sup>J. R. Capadona, T. A. Petrie, K. P. Fears, R. A. Latour, D. M. Collard, and A. J. Garcia, *Adv. Mater.* **17**, 2604 (2005).
- <sup>10</sup>H. Kikuta, H. Toyota, and W. Yu, *Opt. Rev.* **10**, 63 (2003).
- <sup>11</sup>P. B. Clapham and M. C. Hutley, *Nature* (London) **244**, 281 (1973).
- <sup>12</sup>B. MacLeod and G. Sonek, *Laser Focus World* **35**, 109 (1999).
- <sup>13</sup>H. Nakano, H. Morita, H. Washida, T. Kato, S. Hayashi, and A. Onoe, *Opt. Eng.* **24**, 207 (1985).
- <sup>14</sup>B. L. Soporì and R. A. Pryor, *Sol. Cells* **8**, 249 (1983).
- <sup>15</sup>L. Zhuang, S. Schablitsky, R. C. Shi, and S. Y. Chou, *J. Vac. Sci. Technol. B* **14**, 4055 (1996).
- <sup>16</sup>R. Magnusson and S. S. Wang, *Appl. Phys. Lett.* **61**, 1022 (1992).
- <sup>17</sup>R. Magnusson and S. S. Wang, *Appl. Opt.* **34**, 8106 (1995).
- <sup>18</sup>S. Tibuleac and R. Magnusson, *J. Opt. Soc. Am. A* **14**, 1617 (1997).
- <sup>19</sup>J. L. Stay and T. K. Gaylord, *Appl. Opt.* **47**, 3221 (2008).
- <sup>20</sup>S. R. J. Brueck, *Proc. IEEE* **93**, 1704 (2005).
- <sup>21</sup>Y. Liu, S. Liu, and X. Zhang, *Appl. Opt.* **45**, 480 (2006).
- <sup>22</sup>L. Z. Cai, X. L. Yang, and Y. R. Wang, *Opt. Lett.* **27**, 900 (2002).
- <sup>23</sup>Y. Lin, P. R. Herman, and K. Darmawikarta, *Appl. Phys. Lett.* **86**, 071117 (2005).
- <sup>24</sup>L. Wu, Y. Zhong, C. T. Chan, K. S. Wong, and G. P. Wang, *Appl. Phys. Lett.* **86**, 241102 (2005).
- <sup>25</sup>S. Yang, M. Megens, J. Aizenberg, P. Wiltzius, P. M. Chaikin, and W. B. Russel, *Chem. Mater.* **14**, 2831 (2002).
- <sup>26</sup>V. Berger, O. Gauthier-Lafaye, and E. Costard, *J. Appl. Phys.* **82**, 60 (1997).